TENTH AUSTRALASIAN FLUID MECHANICS
CONFERENCE - UNIVERSITY OF MELBOURNE
11-15 DECEMBER 1989

OPEN SEPARATION AND VORTEX FORMATION NUMERICAL SIMULATION AND ANALYSIS OF A DELTA WING FLOW

A. HILGENSTOCK, H. VOLLMERS and U. DALLMANN

DLR - Institute for Theoretical Fluid Mechanics
Bunsenstraße 10

D-3400 Göttingen
WEST GERMANY

In the present investigation we are interested in the determination of so called vortex cores. A numerical analysis of various flow properties associated with the formation of three-dimensional vortices due to flow separation from a round edged delta wing should improve our understanding of three-dimenisonal separated flows in general and could support the aims of predicting flow separation from smooth bodies.

ON THE TOPOLOGICAL DEFINITION OF THREE-DIMENSIONAL FLOW SEPARATION AND VORTEX FORMATION

Many papers have been published in recent years on topics of experimental or numerical visualization of three-dimensional separating flows around blunt or pointed bodies. Qualitative changes in the observed surface flows were recognized to occur due to changes in parameters like Reynolds number, Mach number, angle of attack, body shape, etc. A description of surface flow topology turned out to be a usefull means to reduce the qualitative information provided by the surface flow data (or visualizations) to give a precise description of flow changes in terms of topological changes. However, surface flow trajectories, especially wall shear stress informations are never - even in two-dimensional flow - sufficient to conjecture qualitative features within the outer (mid-air) flow field. Hence, for the formation of a vortex core - (even when a precise definition would allow to locate or define it in mid-air) - a wall shear stress topology in general cannot provide sufficient conditions for a vortex existence. The so called open separation is one such striking example: Although the surface flow topology in terms of the wall shear stress topology on the delta wing considered here or on a prolate spheroid, does not change (for instance) in a wide range of angles of attack separated vortices are, nevertheless, observed on the leeward side of the bodies. (We remind the reader that any, arbitrarily weak or strong convergence of neighbouring wall shear stress trajectories does not cause any topological change of that surface flow). This raises the question whether the onset of such a vortex flow feature - (namely the formation of a localized swirling flow region in mid-air) - can be assigned to a topological change of some other flow quantity. (From an applicational point of view any quantity which leaves a unique "footprint" on the wall (body surface) within measurable quantities would be preferred).

For the time being no such topological property is known. Hence, we undertake a study where topological properties and changes of at least all the dependent variables, of flow field invariants, etc., are investigated. The following discussion is based on first results derived by a direct numerical simulation of the compressible transitional flow around a round edged delta wing at a Reynolds number $Re = 4.5 \times 10^6$, a Mach number $M_\infty = 0.85$ and an angle of attack $\alpha = 10°$ in a Newtonian fluid. (For similar aims the separated flow around a sphere with interest in the Reynolds number dependent changes in the wake and on the sphere surface is under investigation (Dallmann et al. (1989).

For the free stream conditions described, the flow around a delta wing is dominated by a primary vortex separating close to the leading edge of the wing (as is sketched in figure 1). Because of the spanwise pressure gradient a secondary vortex is generated below the primary vortex. Depending on the strength of the secondary vortex, the primary vortex is shifted inboard the wing. For a sharp edged wing the primary vortex starts at the apex of the wing and separates along the leading edge. For the rounded leading edge, however, the primary separation is not fixed at the leading edge, and depends strongly on the geometry of the leading edge, the sweep angle, the transition from laminar to turbulent flow and so forth.

LAMINAR-TURBULENT TRANSITION ON DELTA-WING

One of the earlier experimentally tested configurations was a delta wing-body configuration with a rounded leading edge (Elsenaar et al. (1986)). Wind tunnel tests for this configuration and the desired free stream conditions ($M_\infty = 0.85$, angle of attack $= 10^0$) were carried out at NLR- and DLR-wind tunnels for different Reynolds numbers. The Reynolds number for the NLR experiments was 9×10^6 and for the DLR experiments it was 4.5×10^6 based on the root chord length.

Detailed comparisons between numerical calculations and these experimental simulations were made by A. Hilgenstock [in preparation] in order to better understand some differences observed in the two tests in the measured wall pressure distributions. It turned out that for quantitative rather than qualitative comparisons between the different experiments as well as between experimental and numerical simulation a precise determination of transition location was cruical. When selecting the transition position at 2.5% local chord the agreement between the numerical simulations and the experimental data was good except that the slope of the c_p-distributions close to the attachment line of the primary vortex was not correctly predicted. This can probably be improved by using an adaptive grid generation technique. Because of this finding the transition location for the present investigtion on a similar delta wing without central body has been kept at 2.5% local chord.

NUMERICAL ALGORITHM AND BOUNDARY CONDITIONS

The complete Navier-Stokes equations are integrated with a finite volume four-stage Runge-Kutta method. The turbulent flow calculations are based on the algebraic turbulence model of Baldwin et al. (1978), with modifications after Degani et al. (1983).

The block-structured code of Schwamborn (1988) is completely vectorized for use on CRAY vector computers, and works on one block at a time in core. Each block is thus treated separately in core, and is progressed by one time step, while all other blocks are stored out of core on a storage device with a hyperchannel connection (solid state storage device = SSD). The conditions at the interface of neighbouring blocks are treated in a simple fashion, because the blocks are overlapped at the block boundaries. At the wing surface no-slip conditions are applied, and the normal derivatives for pressure and temperature are set to zero. Other conditions could, of course, be used, e.g. applying the surface normal momentum equation to determine the wall pressure. In the plane of symmetry symmetry conditions are used. At the far field boundary locally one-dimensional Riemann invariants are employed normal to the boundary.

The numerical simulation of the complex three-dimensional flow field around a delta wing requires a mesh with about 1.000.000 node points. For each node point 8 variables like the three cartesian coordinates x, y and z, the three velocity vector components u, v and w, and two skalar values like pressure p and temperature T have to be stored at each grid point, resulting in a data base of 8 Mega words. The interpretation of such a huge data base is done on SUN-graphics work stations with a special graphic program named COMADI by Vollmers (1989). Fig. 2 shows part of the mesh on the wing used for the present calculations. The extrem clustering of grid points near the leading edge was chosen in order avoid possible vorticity generation due to numerical (resolution) errors. The boundary layer along the plane of symmetry has been resolved by up to 30 node points.

RESULTS

A perspective view of the wing starboard side and the leeward vortex flow is shown in figure 3. Since the flow is symmetric (yaw angle = 0) the other side will not be displayed to show the calculated results in fig. 4 to 12.

Skin friction delivers first informations to be analyzed in order to detect flow separation. Skin friction is directly proportional to the surface vorticity which is displayed in fig. 5. One recognizes very strong gradients in regions near the leading edge where the separation lines and the attachment lines are identified in fig. 7. It might be misleading to concentrate one's interests on the skin friction trajectories only because it is the vorticity which drives the flow field. Convergence and divergence of neighbouring skin friction lines are accompanied by changes in vorticity line curvature and strong stretching of vortex tubes above the wing occurs.

Figure 7a shows the numerically simulated skin friction lines, fig. 7b shows a blow up of the region where the primarily separating vortex is formed by a so called open separation. The separation line forms at about 25% root chord on the upper side of the wing surface very close to the leading edge. Skin friction lines which reach the leeward side turning around the leading edge between 0% and 10% root chord do not enter the region below the primary vortex. They stay between the plane of symmetry and a so called primary attachment line. Only the skin friction lines which enter the leeward side between 10% and 25% root chord will be trapped below the primary vortex. These skin friction lines gradually diverge from the primary attachment line and follow strong convergence towards an open primary separation line seen in fig. 7b. At about 70% root chord a secondary flow separation takes place. This is also an open separation, where neighbouring skin friction lines converge and gradually form a separation line which is seen in the left part of fig. 7a.

Unfortunately no explicit criterion is known which allows to determine the location of open separation lines seen in fig. 7 without calculating and analyzing the whole distribution of surface flow streamlines.

For an incompressible two-dimensional flow it has been shown by Dallmann (1985) that only a complete discription of the surface pressure and the wall shear stress leads to a unique, complete description of the flow above the wall. In the present case of a compressible three-dimensional flow the situation is expectedly more complicated. Further theoretical work will be required to better understand the connections between a flow field and its (qualitative) "footprints" detectable in different quantities along the body surface.

Fig. 6 shows the surface pressure distribution which allows a qualitative comparison with skin friction lines or surface vorticity. One recognizes local pressure minima firstly in the downstream region between primary separation and attachment lines and, secondly, in the region where the primary separation lines forms. In a possible continuation of the present study we shall be investigating how the relationship between figs. 4, 5 and 6 changes due to changes of angle of attack (or Reynolds number and Mach number).

Let us now display the vortex flow above the wing. Fig. 4 shows some selected streamlines within the primary vortex. The region of the vortex core is displayed by selected streamlines. Since the streamlines are displayed utilizing a "hidden line algorithm" the direction of rotation can be identified. Looking more into the details, it turns out that streamlines left outside a "vortex core" will not enter that core and core streamlines will not come out of that core. Fig. 3 is an attempt to summarize the essential spatial distribution of selected streamlines which form the "vortex cores". But, how can we define the location of such "vortex cores"?

First let us take an experimentalist's point of view who tries to vizualize such vortex cores. He is asked to visualize a very complicated twisting and folding and perhaps focal winding (Dallmann (1988)) of streamlines and streamsurfaces by a proper selection of initial points where he releases (for instance) smoke. Fig. 3 shows a sketch of what he might observe.

A vortex core is sketched as a bunch of streamlines, and is indicated by number "1". Streamlines indicated by number "2" pass above the separation line, turn around the vortex core and reach the separation line again coming from the plane of symmetry. These streamlines are then again fed into the primary vortex. Streamlines starting near point number "3" turn around the primary vortex and form the secondary vortex under the action of the spanwise pressure gradient.

Light sheet visualization is a means to show the topological velocity field structure within so called Poincaré sections cutting through a flow field (Dallmann et al. (1989) if well defined initial points can be selected where particles are introduced into the flow. In this respect open separation in contrast to closed separation causes severe problems. Fig. 8 shows a plane in front of the wing, where small, inertialess particles are emitted to skatter light for the use of laser sheet visualization technique. These particles are obviously not able to enter the primary vortex core, and so the primary vortex stays black in a laser sheet flow visualization. Only the secondary vortex is filled with particles which can be illuminated. Refering to fig. 3, the secondary vortex is formed of streamlines coming from outside the primary vortex, where fluid particles are present. Fig. 9b shows a photograph of an experimental laser sheet visualization at about 50% root chord (Bütefisch in: Elsenaar et al. (1986)) and Fig. 9a shows our numerically simulated laser sheet at 80% root chord. To illuminate the primary vortex it would be neccessary to eject particles from stations near to the leading edge of the wing between 10% and 25% root chord. This is the only technical possiblity to feed the primary vortex core.

How close to the wing surface all of those vortex core streamlines turn around the leading edge can be conjectured from vortex core streamline integration performed in upstream direction. The integration procedure used on the SUN-graphic workstation breaks down in this narrow region (see fig. 2) because the lines approach the surface. In this region the applied linear interpolation is inappropriate and the integration scheme does not accurately follow the curvature of the direction field.

Let us now turn to an analytical definition of a vortex core. Vollmers (1983) has proposed to locate vortices in regions where the velocity derivative tensor $u_i|_j$ (rate of deformation tensor) exhibits complex eigenvalues and the only one existing real eigenvector defines the local axis of rotation of the fluid as seen by an observer moving with the flow. Vollmers analyzed experimental data of a flow around a prolate spheroid where, similar to the flow investigated in the present paper, open separation leads to the formation of leeside vortices. In addition he investigted the relative orientation of core streamlines, core vorticity lines and the direction of the eigenvector in the regions of complex eigenvalues. Fig. 10 shows this region for the flow around round edged delta wing. We may call this region the vortex core. The findings of Vollmers (1983) and the study of Shirajama (1989) as well as the basic considerations of vortex structures and vorticity field topology by Dallmann (1988) suggest that vortex cores also exhibit regions of strong vortex stretching, by almost parallel alignement of local velocity vector and vorticity vector. A more detailed study of vorticity line advection, spatial concentration, possible reconnection, etc. will be performed.

After having identified primary and secondary vortices other flow quantities like local Mach number, static pressure and total pressure loss will be considered in selected planes normal to the plane of symmetry. Also the core streamlines will be displayed to relate the vortex to local minima and maxima of the above quantities.

Fig. 11 shows the total pressure loss in planes between 50% and 90% root chord. The maximum total pressure loss is aligned with the primary vortex core. The total pressure loss between the wing leading edge and the primary vortex is not everywhere due to the secondary vortex. At 50% root chord this total pressure loss is generated by the outer part of the primary vortex. Looking at a single plane without additional information of core streamlines might be misleading. The static wall pressure and the static pressure in planes between 10% and 90% root chord shows, in combination with the streamlines, that the vortex core is aligned with a local pressure minimum. Although the pressure decreases towards the trailing edge, the footprint of the vortex on the surface shows an almost constant pressure. This is due to the departure of the vortex core which follows approximately a direction of 2.5° away from the wing upper surface at 10° angle of attack.

Fig. 12 shows the Mach number distribution between 10% and 90% root chord. The vortex core, presented by streamlines, is not related to the maximum of the local Mach number, but is rather accompanied by a local minimum. The maximum Mach number value located above the vortex core is due to high mainflow velocity, the maximum below is due to high cross flow velocity.

REFERENCES

BALDWIN, B.S.; LOMAX, H. (1978) Thin Layer Approximation and Algebraic Model for Separated Turbulent Flows. AIAA Paper 78-257, 1978.

DALLMANN, U. (1988) Three-Dimensional Vortex Structures anf Vorticity Topology. Proc. IUTAM Symposium on Fundamental Aspects of Vortex Motion, 31.8.-4.9.1987, Tokyo, Japan, (H. Hasimoto and T. Kambe, eds.), North-Holland Amsterdam, pp.183-189.

DALLMANN, U., SCHULTE-WERNING, B. (1989) Topological Changes of Axisymmetric and Non-Axisymmetric Vortex Flows. Proc. "IUTAM Symposium on Topological Fluid Mechanics", August 13-18, 1989, Cambridge, UK, Cambridge University Press.

DEGANI, D., SCHIFF, L.B. (1983) Computation of Supersonic Viscous Flows Around Pointed Bodies at Large Incidence. AIAA-83-0034, 1983.

DALLMANN, U. (1985) On the Formation of Three-Dimensional Vortex Flow Structures. DFVLR-Report 221-85 A 13.

ELSENAAR, A., ERICSSON, G. (1986) "International Vortex Flow Experiment on Euler Code Validation". Proceedings, Stockholm, October 1-3, 1986 (published by FFA).

SCHWAMBORN, D. (1988) Simulation of the DFVLR-F5 Wing Experiment Using a Block Structured Explicit Navier-Stokes Method. Vieweg Series, Notes on Numerical Fluid Mechanics, Vol. 22.

SHIRAYAMA, S. (1989) A Structure of Leading-Edge and Tip Vortices at a Delta Wing. AIAA-CP 89-1803.

VOLLMERS, H. (1989) A Concise Introduction to COMADI. DFVLR-Report 222-89 A22.

VOLLMERS, H. (1983) Separation and Vortical-Type Flow around a Prolate Spheroid. Evaluation of Relevant Parameters. AGARD-CP 342, pp.14-1 – 14-14.

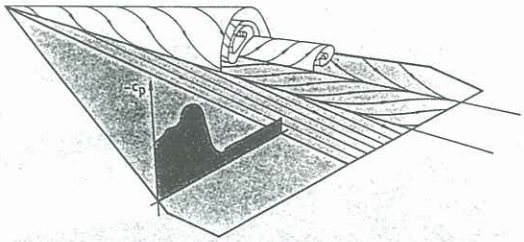

Fig. 1 Principle sketch of vortex flow

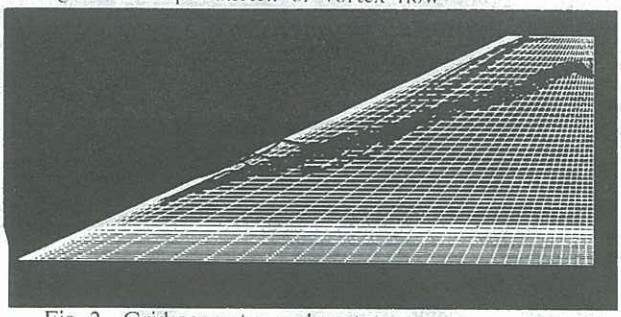

Fig. 2 Grid geometry and vortex core

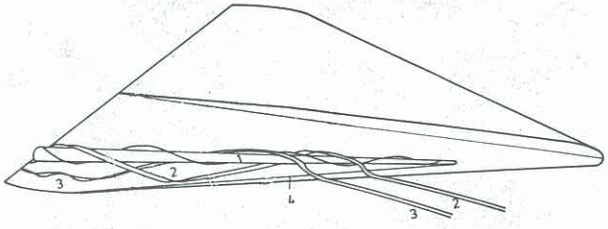

Fig. 3 Sketch of primary and secondary vortex

Fig. 4 Vortex flow displayed by streamlines

Fig. 5 Surface vorticity distribution

Fig. 6 Surface pressure distribution

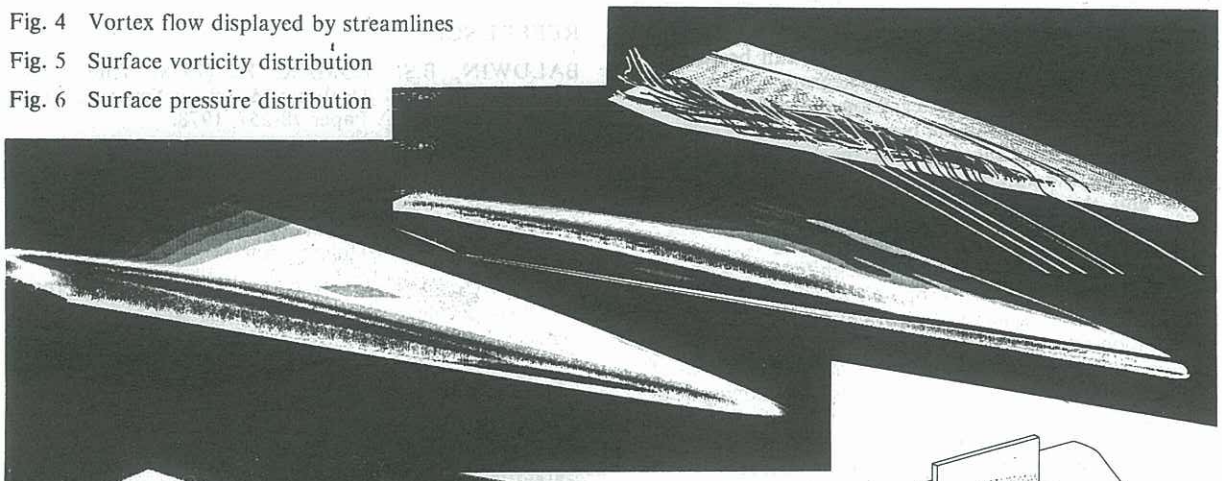

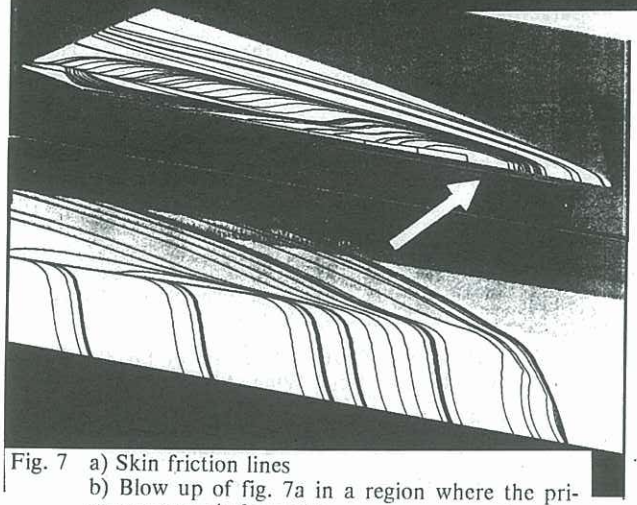

Fig. 7 a) Skin friction lines
b) Blow up of fig. 7a in a region where the primary vortex is formed by an open separation

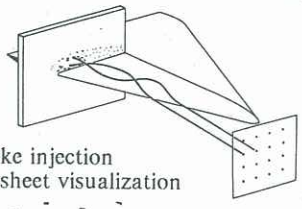

Fig. 8 Sketch of smoke injection for laser light sheet visualization

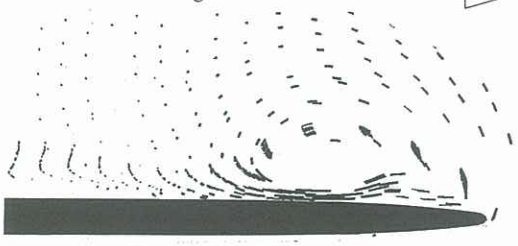

Fig. 9 a) Numerical simulation of light sheet visualization at 80% root chord
b) Experimental laser light sheet visualization on a delta wing at 50% root chord

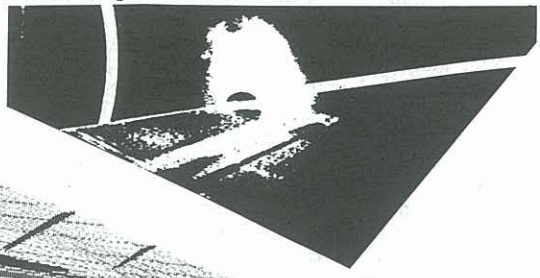

Fig. 10 Vortex core identified by regions of complex eigenvalues of the rate of deformation tensor

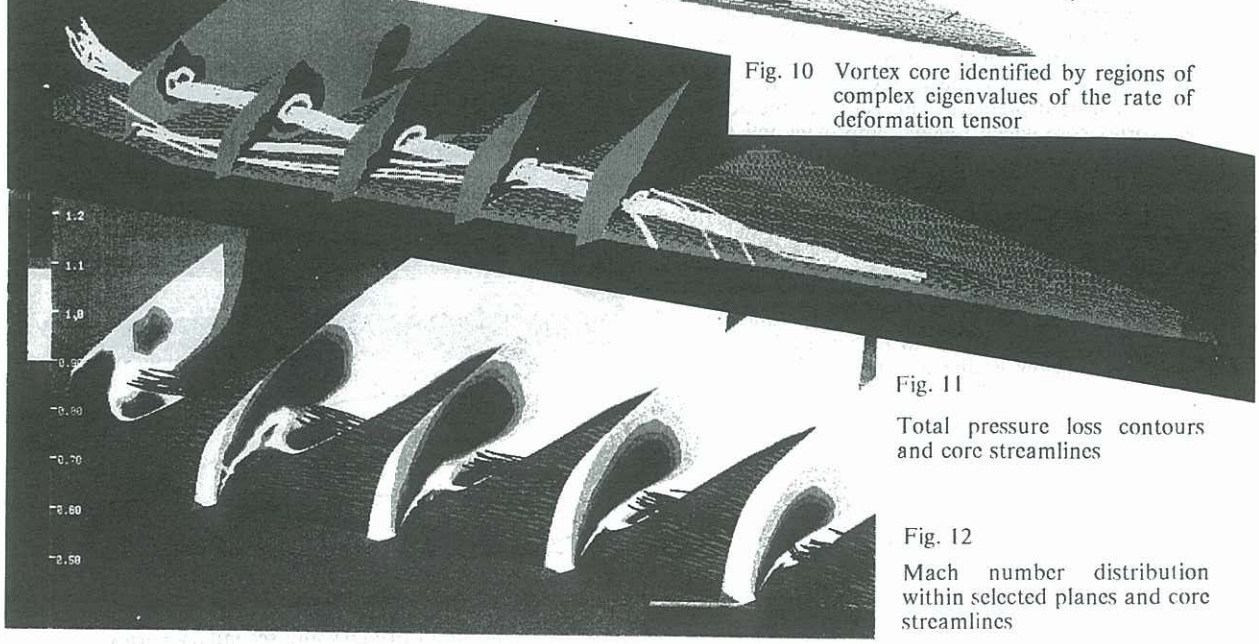

Fig. 11

Total pressure loss contours and core streamlines

Fig. 12

Mach number distribution within selected planes and core streamlines